processes

MDPI

Article

Influence of Porous Media Aperture Arrangement on CH_4/Air Combustion Characteristics in Micro Combustor

Fei Wang [1,2], Xueming Li [1,*], Shuai Feng [3] and Yunfei Yan [3,*]

[1] College of Chemistry and Chemical Engineering, Chongqing University, Chongqing 401331, China; wf20023184@163.com
[2] Chongqing Special Equipment Inspection and Research Institute, Chongqing 401121, China
[3] Key Laboratory of Low-Grade Energy Utilization Technologies and Systems, Chongqing University, Ministry of Education, Chongqing 400030, China; shuaifengcqu@cqut.edu.cn
* Correspondence: xuemingli@cqu.edu.cn (X.L.); yunfeiyan@cqu.edu.cn (Y.Y.)

Abstract: Micro-electro-mechanical systems (MEMS) occupy an important position in the national economy and military fields, and have attracted great attention from a large number of scholars. As an important part of the micro-electromechanical system, the micro-combustor has serious heat loss due to its small size, unstable combustion and low combustion efficiency. Aiming at enhancing the heat transfer of the micro-combustor, improving the combustion stability and high-efficiency combustion, this paper embedded porous media in the combustor, and the effects of different parameters on the combustion characteristics were numerically studied. The research results showed that the layout of porous media should be reasonable, and the small and large pore porous media embedded in the inner and outer layers, respectively, can bring better combustion performance. Meanwhile, A: 10–30 has a high and uniform temperature distribution, and its methane conversion rate reached 97.4%. However, the diameter ratio of the inner layer to the outer layer (d/D) of the porous medium should be maintained at 0.4–0.6, which brings a longer gas residence time, and further enables the pre-mixed gas to preheat and burn completely. At a d/D of 0.5, the combustor has the highest outer wall temperature and CH_4 conversion efficiency. Besides, compared with the pore size increasing rate of Δn = 10 PPI and Δn = 10 PPI, the radial temperature distribution of the Δn = 10 PPI combustor is more uniform, meanwhile avoids the occurrence of local high temperature. Under the condition of Δn = 10 PPI, A: 20–30 layout maintains excellent thermal and combustion performance. In addition, the lean flammable limits of MC-U20, MC-10/30-0.8, and MC-20/30-0.5 were compared, at an inlet velocity of 0.5 m/s, the corresponding lean flammable limits are 0.5, 0.4, and 0.3, respectively, among them MC-20/30-0.5 has a wider flammable limit range, showing excellent combustion stability. This research has guiding significance for the combustion stability of the micro combustor.

Keywords: micro combustor; porous media; PM layout; PM d/D; increase rate; lean flammable limit

Citation: Wang, F.; Li, X.; Feng, S.; Yan, Y. Influence of Porous Media Aperture Arrangement on CH_4/Air Combustion Characteristics in Micro Combustor. *Processes* **2021**, *9*, 1747. https://doi.org/10.3390/pr9101747

Academic Editor: Zhihua Wang

Received: 14 September 2021
Accepted: 28 September 2021
Published: 29 September 2021

1. Introduction

Microelectromechanical systems (MEMS) have broad application prospects in the national economy and military fields, especially in the fields of electronics, medicine, industry, automobiles, and aerospace systems [1–3]. Nowadays, the energy supply of these devices comes from traditional chemical batteries, which are limited by traditional chemical batteries, including factors such as small energy density, large volume, and long charging time, making it difficult to achieve high energy density requirements [4–7]. Fortunately, hydrogen and hydrocarbon fuels have a high energy density, and the typical liquid hydrocarbons can reach 45 MJ/kg, while the energy density of commonly used lithium batteries is only 1.2 MJ/kg. Thus, as long as stable and efficient combustion can be maintained, micro-electromechanical systems based on combustion have great application potential [8–10]. The micro combustor is a critical component of the micro power system, but due to the drastically decrement in size of the micro combustor, the area-to-volume ratio of the combustion chamber is drastically

increased, resulting in serious heat loss. In addition, the reduced residence time of the fuel in the combustor leads to insufficient combustion and non-uniform temperature distribution, resulting in low combustion efficiency and increased pollutant emissions [11,12]. Therefore, it is very necessary to adopt effective measures to improve the combustion efficiency and stability in the micro combustor, and to optimize the temperature distribution.

In recent years, related scholars have conducted a lot of researches and obtained results in the structure of micro-combustor and flame stabilization technology. From the perspective of catalytic combustion, Li [13] proposed a platinum-plated asymmetric flat plate micro-combustor and studied the thermal characteristics of non-premixed CH_4/air catalytic combustion. The study found that combustion can occur at an average inlet velocity above 9 m/s, and the maximum combustion efficiency and surface radiation efficiency reached 98.5% and 25.9%. Wu [14] proposed a multi-stage separated baffle cylindrical micro-combustor with platinum-plated catalyst inside, and compared it with a traditional cylindrical combustor. It was found that the combination of multi-stage baffle and catalyst significantly improved the combustion efficiency and flammability limit of the combustor. Pan [15] studied catalytic combustion of hydrogen/air in a plate combustor using a combination of experimental and numerical studies. Compared with traditional combustion (without catalyst plating), the flammability limit of combustion is broadened. There are many researches using this kind of similar catalytic combustion, and it has certain positive effect on improving the combustion stability [16–23]. However, it should be noted that catalysts still have problems of failure, especially under long-term high temperature conditions. Therefore, a large number of scholars from the combustor structure design, the use of cavity and blunt body reflux zone for stable combustion. Zuo [24] designed a cylindrical combustor with a concave cavity, and studied the effects of inlet velocity, equivalent ratio, and materials. The results showed that compared with the traditional cylindrical combustor (without cavity), its thermal performance is significantly improved, and the average outer wall temperature reaches 1306.88 K. Gao [25] proposed a micro combustor with cavity and guide vane, and compared its combustion characteristics. It is found that the combustion efficiency and thermal characteristics are improved obviously, with an inlet velocity of 32 m/s, the combustion efficiency is increased by 85.96%, and the reaction heat reaches 244.5 W. Similarly, Xu [5] combined the stable combustion characteristics of the cavity and the blunt body, and carried out a slit treatment in the center of the blunt body. The study showed that it can prolong the residence time of fuel and improve the combustion stability. Su [26] proposed a micro combustor with double cavities and studied its thermal characteristics. The results showed that the existence of double cavity brings a higher and uniform temperature distribution of the outer wall, meanwhile improves the radiation efficiency. Yang [27] adopted a cavity design to broaden the blowing limit of the flame, and found that the cavity can improve the combustion efficiency and improve the flame tip splitting phenomenon. He [28] and other relevant scholars have conducted a large number of studies to prove the steady burning effect of blunt body, especially in improving combustion efficiency, making the application of cavity and blunt body in micro combustors reach a high level [29–34].

Now, more and more scholars from the perspective of thermal management, are adopting measures to reduce heat loss, so as to pursue efficient and stable combustion. This method mainly uses heat recirculation to reduce heat dissipation loss, let high temperature exhaust preheat low temperature gas, improve the inlet gas temperature to stabilize combustion. He [35] proposed a U-shaped heat recirculation combustor, which uses baffles to isolate the combustion zone from the preheating zone and preheats through the baffles. It is found that heat recirculating is beneficial to increase the methane conversion rate and improve stable combustion. Similarly, Tang [36] designed a flat U-shaped combustor and studied the energy conversion efficiency of the entire micro-thermal photovoltaic system (MTPV). It is found that compared with the traditional straight-channel micro-combustor, its energy conversion efficiency has doubled. In addition, a large number of studies have shown that the heat recirculation combustion technology has better thermal performance,

and it can be used to enhance combustion at a small scale [37–41]. As an excellent thermal management method, porous media combustion has also received extensive attention from scholars, because the gas has a strong coupling effect with the porous medium during the combustion process, it can strengthen the overall combustion reaction and improve the combustion efficiency. Wu [42] studied the thermal characteristics of micro-combustors embedded with porous media and found that SiC is an excellent porous media material, and Al_2O_3 is more suitable as a combustor wall material. The maximum output power of the system reaches 3.10 W when the equivalence ratio is 0.9. Ni et al. [43] proposed to embed Y-type and T-type combustors in porous media, and studied their energy conversion efficiency. It is found that the porous media embedding improves the temperature uniformity of the outer wall, meanwhile improves the energy conversion efficiency of the overall system. Peng et al. [44] experimentally studied the heat transfer characteristics of the embedded porous medium combustor, and analyzed the influence of the porous medium material and the porosity. It was found that the pore ratio of 0.9 showed the highest average outer wall temperature and maintained excellent temperature uniformity. Xie [45] studied the thermal characteristics of multilayer porous media combustors through experiments and numerical methods, and found that compared with uniformly arranged porous media, the thermal characteristics of the three-layer layout are better, which is beneficial to increase the output power. Li [46] used experiments to study the dynamic flame behavior in a porous media micro combustor, and analyzed the effects of the embedding position, width and porosity of the porous media. The results showed that reasonable parameter selection can improve the thermal performance of the combustor.

The above related researches shows that the porous medium combustion technology has shown great advantages in the combustion stability, combustion efficiency, combustion limit and pollutant emission of the micro combustor, especially the reasonable layout of the porous medium [47–50]. It can be seen that porous media has a positive effect on combustion stability and enhanced heat transfer, the key issue for its restricted applications is the reasonable layout of porous media. Therefore, this paper proposes to embed porous media in a micro-combustor, and reasserted the effects of porous media layout, interlayer diameter ratio (d/D), pore size increase rate, and lean flammability limit, so as to provide a basis for the design of porous media in the micro combustor.

2. Numerical Model

2.1. Physical Model

As shown in Figure 1, the micro combustor is composed of a front inlet part and a combustion chamber, the inlet part is an annular inlet, and the combustion chamber is filled with foam ceramic porous medium. The premixed methane/air enters the combustor from the inlet, combustion occurs in the chamber and is discharged as exhaust gas through the outlet. The annular inlet has an inner diameter (d_1) of 8 mm and an outer diameter (d_2) of 12 mm, maintaining a length of 5 mm. The combustion chamber is a cylindrical chamber with a total length (L) of 60 mm, an outer wall diameter (d_3) of 20 mm, and an outer wall thickness (δ) of 1 mm. The ceramic foam porous medium is located in the middle of the combustion chamber, with an inlet gap (L_1) of 5 mm and an outlet gap (L_2) of 3 mm, the inner and outer porous media have different porosities, and the corresponding outer diameters d and D are variable.

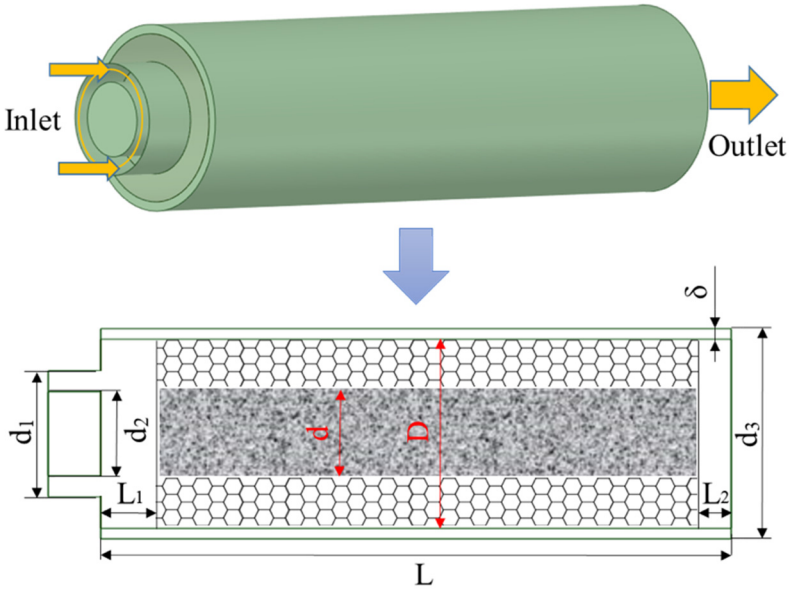

Figure 1. Schematic diagram of geometric structure.

2.2. Mathematical Model

Since the cylindrical model selected in this paper is a three-dimensional center symmetric structure, for saving computer resources, only its two-dimensional structure is calculated. For the convenience of calculation, assumptions are made on the research conditions related to the model. The radiation effect of gas is ignored and the effect of viscous force is not considered, the embedded porous media is regarded as an inert porous media, and the gas and solid are in a heat balance state. The relevant control equations involved in this paper are as follows:

Continuity equation:

$$\frac{\partial(\varepsilon\rho U)}{\partial x} + \frac{\partial(\varepsilon\rho V)}{\partial y} = 0 \tag{1}$$

Momentum equation:

$$\frac{\partial(\varepsilon\rho UU)}{\partial x} + \frac{\partial(\varepsilon\rho UV)}{\partial y} = -\frac{\partial P}{\partial x} + \frac{\partial}{\partial x}(\mu\frac{\partial U}{\partial x}) + \frac{\partial}{\partial y}(\mu\frac{\partial U}{\partial y}) + \frac{\Delta P}{\Delta x} \tag{2}$$

$$\frac{\partial(\varepsilon\rho UV)}{\partial x} + \frac{\partial(\varepsilon\rho VV)}{\partial y} = -\frac{\partial P}{\partial y} + \frac{\partial}{\partial x}(\mu\frac{\partial V}{\partial x}) + \frac{\partial}{\partial y}(\mu\frac{\partial V}{\partial y}) + \frac{\Delta P}{\Delta y} \tag{3}$$

Energy equation:

$$\begin{aligned}\frac{\partial(\varepsilon\rho UH)}{\partial x} + \frac{\partial(\varepsilon\rho VH)}{\partial y} &= \frac{\partial}{\partial x}(k_{eff}\frac{\partial T_g}{\partial x}) + \frac{\partial}{\partial y}(k_{eff}\frac{\partial T_g}{\partial y}) + \varepsilon\sum_{i=1}^{N} h_i w_i W_i \\ -\varepsilon\frac{\partial}{\partial x}\left[\rho g\sum_{i=1}^{N} Y_i h_i D_{im}\frac{\partial(\rho g Y_i)}{\partial x}\right] &- \varepsilon\frac{\partial}{\partial y}\left[\rho g\sum_{i=1}^{N} Y_i h_i D_{im}\frac{\partial(\rho g Y_i)}{\partial y}\right]\end{aligned} \tag{4}$$

Species transport equation:

$$\frac{\partial(\varepsilon\rho M_i)}{\partial t} + \frac{\partial(\varepsilon\rho UM_i)}{\partial x} + \frac{\partial(\varepsilon\rho VM_i)}{\partial y} = \frac{\partial}{\partial x}\left[\varepsilon D_{im}\frac{\partial(\rho M_i)}{\partial x}\right] + \frac{\partial}{\partial y}\left[\varepsilon D_{im}\frac{\partial(\rho M_i)}{\partial y}\right] + \varepsilon M_i W_i \tag{5}$$

Ideal gas state equation:

$$P = \rho RT\sum_{n=1}^{\infty}\frac{M_i}{M} \tag{6}$$

For the convenience of this study, the relevant physical parameters are defined. Equivalent ratio refers to the ratio of the actual CH_4/Air reaction mass ratio to the theoretical complete reaction mass ratio, which is defined as follows:

$$\phi = \frac{(F/A)_{actual}}{(F/A)_{\text{theory}}} \tag{7}$$

where F is the methane mass fraction and A is the air mass fraction.

In the application of porous media combustion technology, the pore size Reynolds number proposed by Pedras et al. [51,52] is used to define the flow pattern.

$$\text{Re} = \frac{UD}{\gamma} \tag{8}$$

where U represents the average cross-sectional velocity, D and γ represent the average diameter of the porous medium and the viscosity of the fluid, respectively.

The porosity ε = 0.85 and PPI = 25 of porous media materials are selected, and the formulas of viscous drag coefficient C_1 and inertia drag coefficient C_2 are calculated using the empirical formula summarized by Ma [53]:

$$C_1 = \frac{150(1-\varepsilon)n^2}{0.0254^2\varepsilon^3} \tag{9}$$

$$C_2 = \frac{1.75n\sqrt{1-\varepsilon}}{0.0254\varepsilon^3} \tag{10}$$

The methane conversion efficiency of the micro combustor in this paper can be defined as follows:

$$\eta = \frac{\mathrm{m}_{in} - \mathrm{m}_{out}}{\mathrm{m}_{in}} \tag{11}$$

The mass fraction at the inlet of methane is set as m_{in}, and the mass fraction at the outlet is set as m_{out}.

2.3. Boundary Conditions

Compared with the molecular free path of the gas, the micro combustor maintains a large characteristic dimension, and CH_4/air premixed gas can be regarded as an impressible and continuous flow [54]. Kuo [55] suggested that the turbulence model is more suitable for micro-scale combustion when Re > 500, and researchers [56] found that the Realizable k-ε turbulence model is more suitable for turbulent combustion. In this paper, the flow pattern in a porous media combustor is determined by the aperture Reynolds number (Re), and the minimum Reynolds number in this study exceed 500, thus Realizable k-ε turbulence model is selected and the solid–fluid contact walls are coupling boundary conditions. Inlet velocity boundary conditions is applied, while outlet is set as pressure outlet, and the inlet temperature is fixed at 300 K, the outlet gauge pressure is set at 0. For getting close to the real situation, the heat transfer condition of the outer wall is set as mixed heat transfer, and the mixed heat transfer of radiation and convection is considered. The heat transfer expression is:

$$q = h_c(T_W - T_\infty) + \varepsilon\sigma(T_W^4 - T_\infty^4) \tag{12}$$

where T_w and T_∞ represent the wall temperature and environmental temperature (300 K), respectively, and h_c represents convection heat transfer coefficient of 20 W/(m^2·K). While ε and σ represent the wall emissivity (0.8) and the Stephan–Boltzman constant (5.67×10^{-8} W/(m^2·K^4)), respectively. For judging the convergence of the calculation, the residues of continuity, energy, and velocities are monitored, where the standard energy equation for convergence is less than 10^{-6}, and other residual parameters are set at 10^{-3}. The chemical reaction mechanism includes 23 components and 39 steps of elementary reaction, which provides a guarantee for the combustion reaction.

2.4. Numerical Simulation Verification

In order to discretize the calculation area, according to the above assumptions, the three-dimensional problem studied is transformed into a two-dimensional steady-state problem for processing. According to the geometric model mechanism of the porous medium micro-combustor, using Gambit 2.4.6 to draw a two-dimensional axisymmetric mesh as shown in Figure 2.

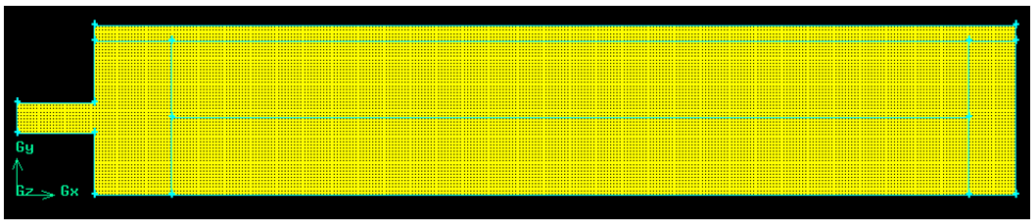

Figure 2. Schematic diagram of micro-combustor mesh.

The mesh size will affect the numerical calculation results, too large a mesh size will increase the calculation error, but a small mesh size will increase the truncation error and calculation resources. However, in order to ensure the calculation accuracy and save the calculation time, the calculation results of the combustor were verified for mesh independence, as shown in Figure 3, the mesh size of 0.05 mm, 0.1 mm, and 0.2 m is selected for calculation, and the results are analyzed for the temperature of the combustor wall. Compared with the mesh size of 0.20 mm, the average outer wall temperature difference of 0.05 mm remains 18.23 K with an error of 1.27%, but the grid size is 0.1 mm and the average wall temperature difference is only 5.26 K, and the error is 0.35%. Therefore, this paper selected 0.1 mm for mesh division, and the result is considered to meet the requirements of mesh independence.

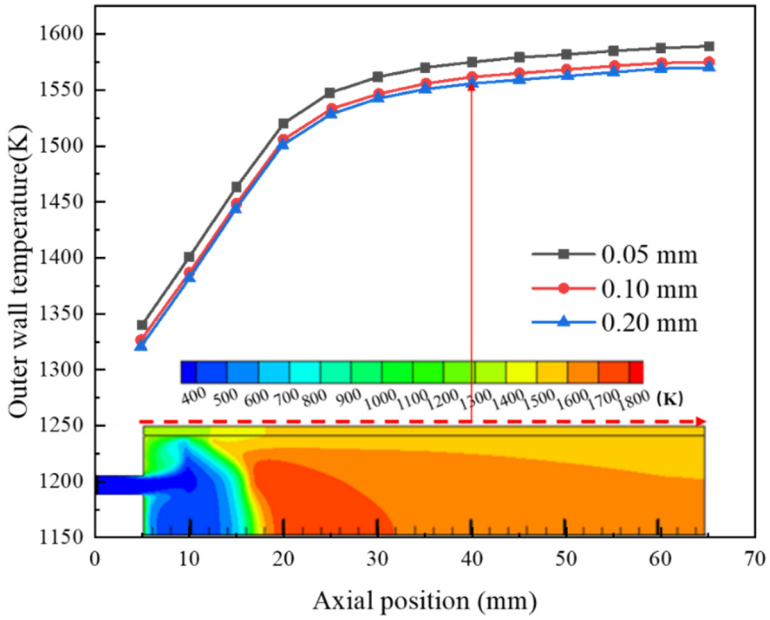

Figure 3. Mesh independence verification.

The rationality of the numerical simulation is based on the accuracy of the results, and the numerical calculation results are compared with the experimental results [57] to verify the accuracy of the model (Figure 4). The same geometric model as the experiment was established, the outer and inner diameters of the combustor were 50 mm and 40 mm, respectively, the length was controlled at 200 mm, and the ceramic plate with a straight

hole of 0.9 mm was embedded. Using the mathematical model of this paper, the numerical calculation is carried out under the equivalence ratio of $\phi = 1.07$, and the outer wall temperature in the numerical simulation is compared with the experimental results. As shown in Figure 4, the temperature distribution of the experimental results and the numerical results are basically consistent, the maximum temperature difference is 142.43 K, with an error of 9.12%, and the average temperature difference is 61.28 K, with an error of 4.05%. As the numerical simulation is under adiabatic conditions and the temperature is slightly higher, this indicates that the mathematical models in this article are feasible.

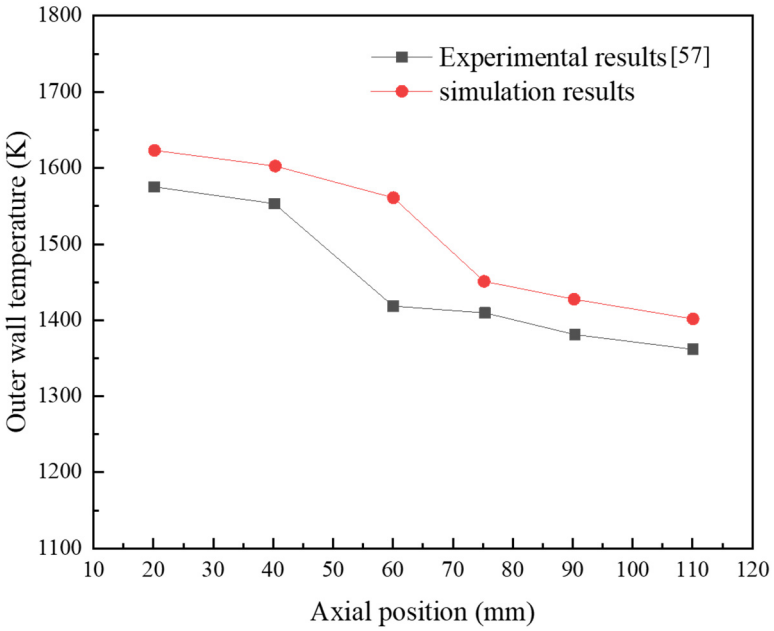

Figure 4. Numerical and experimental verification.

3. Results and Discussion

3.1. Effect of PM Layout

In order to study the influence of the porous media layout on the combustion characteristics, three porous media layouts were selected. The first type is a porous media area with a uniform pore density of 30 PPI, which can be expressed as A: 30-30. The second is the layout of 30 PPI in the outer layer porous media and 10 PPI in the inner layer porous media, expressed as A: 10-30. The third layout of porous media is opposite to the second, which is expressed as A: 30-10.

The outer diameter ratio d/D of the inner layer and outer layer porous media is 0.5, the inlet velocity is controlled to 2 m/s, and the equivalent ratio is set to $\phi = 1$, and the temperature distribution of the three combustors is shown in Figure 5. It can be seen from the temperature distribution that A: 10-30 has the largest entire high-temperature area (temperature higher than 1600 K), followed by A: 30-10, and A: 30-30 has the smallest high-temperature area. It shows that the large outer aperture of PM has obvious advantages, which will bring a more uniform highest temperature area (temperature higher than 1700 K). A: 10-30 occupies almost 80% in the radial direction, while the temperature uniformity of A: 30-10 and A: 30-30 is relatively poor, and the highest temperature area only occupies 40% in the radial direction. This is because the density of large-pore porous media is small, it brings a smaller coefficient of inertial resistance and viscous resistance, which further reduces the pressure of gas flowing in its area. Therefore, in the layout of porous medium with a large pore size at outer layer and a small pore size at inner layer, a smaller flow resistance is brought to the outer layer, meanwhile increase the flow resistance at the inner layer. Under this condition, more gas flows from the outer layer to increase the flow rate, leading gas flow rate in the radial direction tends to be uniform, and the combustion flame

and high temperature area more uniformly along the radial direction. on the contrary, a layout of small pores in the outer layer and large pores in the inner layer is once formed, this aggravates the non-uniformity of the radial flow rate, and the gas flow rate in the inner layer is faster, causing the combustion flame and the high temperature area to be concentrated in the inner layer.

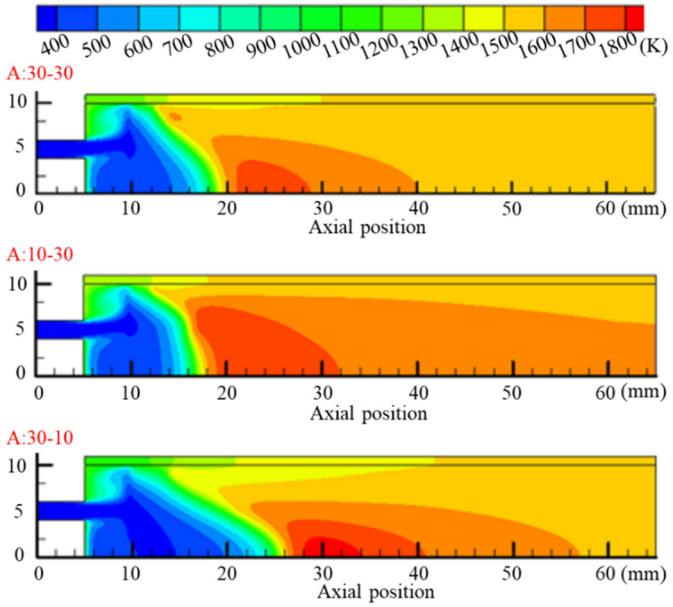

Figure 5. Temperature cloud diagrams with different layouts.

Figure 6 shows the wall temperature of three different layouts of the inner and outer porous media. The wall temperature of different layouts varies similarly with the axial distance, and the wall temperature gradually increases with the progress of the combustion reaction. The wall temperature is mainly judged by the wall temperature of the area after the combustion is stable, it can be seen from the figure that A: 10-30 maintains the highest wall temperature, followed by A: 30-30, and A: 30-10 has the lowest wall temperature. It can be seen that the PM layout in the micro combustor is very critical, a large pore size porous medium is set in the outer layer, and the inner layer maintains a small pore size, which is more reasonable. This is also directly related to the radial temperature distribution in the high temperature area, a uniform radial combustion flame and high temperature area will bring about a higher wall temperature, which is consistent with the previous conclusions.

Combustion requires maintaining a high methane conversion efficiency, and the embedding of porous media also has a greater impact on the methane conversion efficiency, especially the layout of the porous media. Therefore, the methane conversion efficiency under different layout conditions is studied, and the methane conversion efficiency of different combustors is shown in Figure 7. It can be seen from the figure that the methane conversion rates of the three different layouts are relatively high, among them the A: 10-30 maintains the highest conversion efficiency of 97.4%, which is still higher than the 95.3% of A: 30-10 and 96.6% of A: 30-30. Therefore, it can be concluded from the above discussion that the outer layer adopts a large pore size porous medium and the inner layer adopts a small pore size layout, which can improve the flow characteristics in the combustor, resulting in a more uniform temperature distribution and further improving the methane conversion rate.

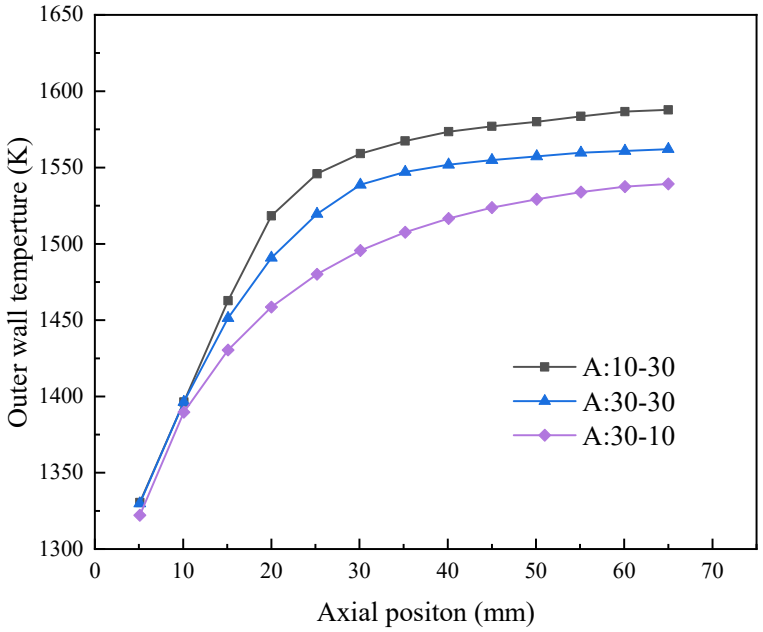

Figure 6. Wall temperature of three different PM layouts.

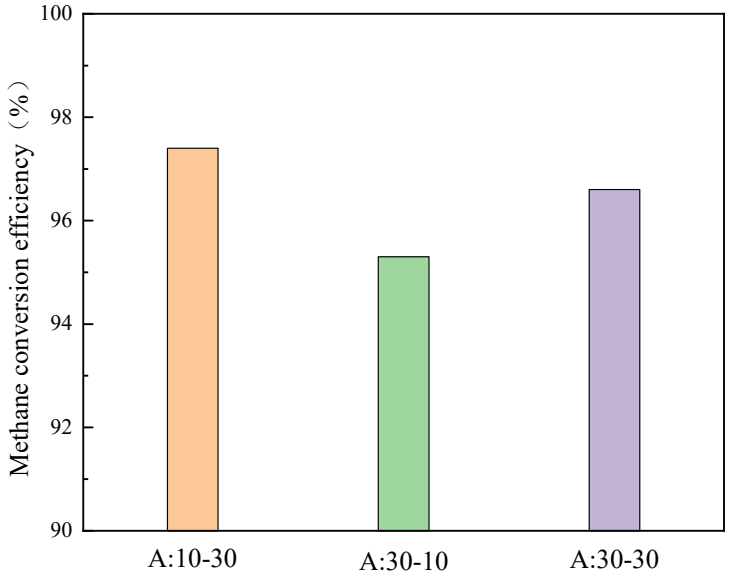

Figure 7. Methane conversion efficiency of different combustor.

3.2. Effect of d/D in Porous Media

In the previous work, the layout of the radial aperture of the double-layer porous medium of the combustor was studied, and the optimal layout of A: 10-30 is obtained. Another very important structural parameter is the thickness ratio of the inner layer and outer layer porous media, which can be evaluated by the outer diameter ratio d/D. Based on this, the temperature distribution with d/D increasing from 0.1 to 0.9 is studied, the outer layer pore density is controlled to 10 PPI, the inner layer pore density is 30 PPI, the inlet velocity v = 2 m/s, and the equivalence ratio is $\phi = 1$.

As shown in Figure 8, it is the temperature distribution diagram of the combustor under different d/D conditions. According to the distribution characteristics of the high temperature area, the influence of d/D can be roughly divided into three stages: axial expansion (d/D: 0.9–0.7), uniform change (d/D: 0.6–0.4) and temperature decrease (d/D: 0.3–0.1). In the range (d/D: 0.9–0.7), the temperature distribution of the combustor is basically the same in the axial direction, the changes are mainly concentrated in the

axial expansion, with the decrease of d/D from 0.9 to 0.7, the high-temperature region gradually stretches downstream in the axial direction. Within the range (d/D: 0.6–0.4), the temperature distribution of the combustor remains consistent regardless of whether it is in the axial or radial direction, and the highest temperature area (greater than 1800 K) disappears, demonstrating a good temperature distribution uniformity. When d/D is less than 0.4 (d/D: 0.3–0.1), the temperature distribution of the combustor decreases, especially when d/D is less than 0.1, all high-temperature regions basically disappear. Analyzing the reasons for the above phenomenon, along with the decrease in the outer diameter ratio d/D, it indicates that the outer large-pore porous medium occupies an increase in the channel area. This increases the flow velocity in the area close to the wall, thereby bringing a more uniform gas flow velocity in the radial direction, and further leading to better temperature uniformity. However, as d/D is further reduced to 0.3, the outer large-pore porous medium almost occupies the entire combustion channel, and the large pore diameter increases so that the inertial resistance coefficient and the viscous resistance coefficient of the porous medium combustion zone are reduced. The preheating effect of the porous medium is reduced, and meanwhile the residence time of the gas is shortened, as a result of incomplete combustion, it will be discharged from the combustion area, which greatly reduces the amount of heat generated by combustion, this is also the reason for the relatively low combustion temperature. Therefore, the high temperature area is uniformly distributed in the range of outer diameter ratio (d/D: 0.4, 0.5, 0.6), and it is considered that the best outer diameter ratio d/D of 0.4–0.6.

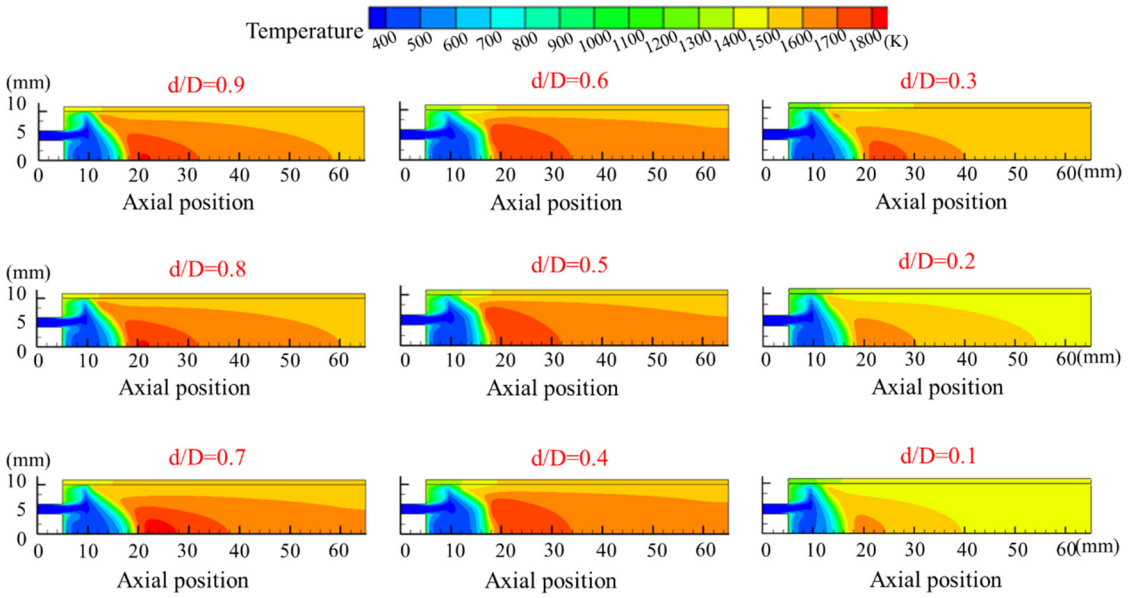

Figure 8. The temperature of different d/D porous media in combustor.

Figure 9 shows the wall temperature distribution of the combustor with different porous media outer diameter ratio d/D. On the whole, the outer wall temperature of different micro combustors is similar, and they all maintain a trend of increasing first and then remaining stable. However, careful analysis shows that the outer wall temperature is not linear with d/D, and there is an optimal value. When d/D increases from 0.1 to 0.5, the outer wall temperature increases as a whole, and the trend is the same, but as d/D continues to increase to 0.9, the outer wall temperature no longer increases but decreases. It can be seen that when d/D is 0.5, that is, when the thickness of the large-pore and small-pore layer is the same, the heat transfer capacity is the best.

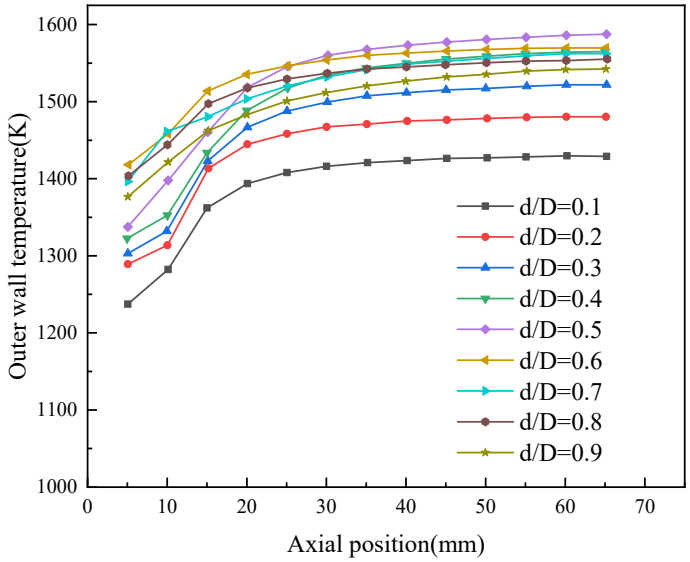

Figure 9. Wall temperature of different d/D porous media.

Figure 10 shows the conversion rate of methane under different d/D conditions. With the increase of d/D from 0.1 to 0.9, the methane conversion rate increased first and then decreased, the conversion rate of d/D reaches a relatively high level in the range of 0.4–0.6. When d/D is 0.4, 0.5, 0.6, the corresponding methane conversion rates are 97.99%, 98.33%, and 97.30, respectively. With a d/D of 0.5, the conversion rate of methane reaches the optimal value at this time, indicating that the methane has been fully burned, which is consistent with the conclusions obtained from the previous temperature distribution. Analysis of the reason: when d/D is too small, it indicates that the combustor is basically occupied by the large-pore porous medium, and the flow resistance is reduced so that the methane is discharged out of the combustor without complete combustion, which reduces the conversion efficiency. However, when d/D is too large, it is also not conducive to the combustion of methane. On the contrary, the porous medium inside the combustor is too dense, and the resistance and pressure are too high. It obstructs the radial flow of methane, but makes the combustion area concentrated in the middle position, and this is difficult to achieve full combustion of methane near the wall. Therefore, a d/D of 0.5 is considered a reasonable choice.

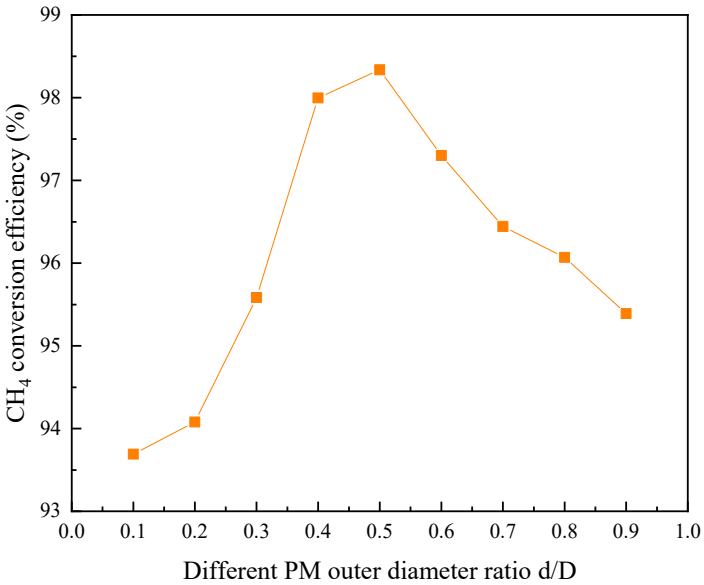

Figure 10. CH_4 conversion efficiency with different d/D porous media.

3.3. Effect of Porosity Gradient

It is known from previous studies that it is more reasonable to fill the large porosity PM at the periphery of the combustor and to set the small porosity PM in the center, and the diameter ratio d/D of the outer PM and the center PM should be maintained at 0.5. However, the porosity gradient in the pore diameter of the inner PM to the outer PM requires further research to obtain. Therefore, in order to study the porosity gradient between the different porous media layers, the following definitions are made:

$$\Delta n = n_w - n_c \quad (13)$$

where n_w represents the void density of the outer large porosity porous medium, and n_c represents the central small porosity porous medium.

In order to explore the influence of different increase values (Δn), three different Δn are set in this article, namely 10 PPI, 20 PPI and 30 PPI. At Δn = 10 PPI, set the four layouts as A: 10-20, A: 20-30, A: 30-40, A: 40-50, at Δn = 20 PPI, set four layouts from A: 10-30, A: 20-40, A: 30-50, A: 40-60, and at Δn = 30 PPI, set two layouts as A: 10-40 and A: 20-50. Other settings are the layout of the porous media with a larger porosity at outer layer and a smaller porosity at inner layer, the outer diameter ratio of the inner layer and outer layer porous media is d/D = 0.5, the inlet velocity v = 2 m/s, and the equivalent ratio is ϕ = 1. Figure 11 is the temperature distribution cloud diagram of different Δn, as shown in Figure 11a, with a Δn of 30 PPI, the overall temperature distribution of the micro-combustor is relatively uniform, but it brings a lower temperature. Meanwhile, the wall temperature of the combustor does not exceed 1500 K, and the maximum temperature remains at about 1600 K. This is because although the optimal value of d/D (0.5) is selected, due to the large gap between different porous media layers, the sudden change in the pore size of the outer porous media is too large, so that the gas is quickly discharged in the outer porous media, and the heat transfer is not sufficiently enhanced.

Based on the above analysis, the aim is to choose a smaller Δn to enhance heat transfer and make the temperature distribution more uniform, selected Δn as 10 PPI and 20 PPI for calculation. Figure 11b shows the temperature distribution of the combustor when Δn is 10 PPI and 20 PPI, respectively. Comparing the temperature distribution of Δn = 10 PPI and Δn = 20 PPI combustors, it is found that when Δn = 10 PPI, the combustor temperature distribution is high and uniform, especially at the most concerned combustor wall position. It can be seen that it is more reasonable to choose Δn = 10 PPI, and it will bring a better outer wall temperature. In order to further obtain the optimal layout under the condition of Δn = 10 PPI, the temperature distributions of four groups of different layouts are compared. Comparing the temperature distribution, it can be seen that the radial temperature gradient of A: 10-20 is relatively large, and the wall temperature is relatively low. However, the temperatures of A: 20-30 and A: 30-40 are high and uniform, especially A: 20-30 has an excellent temperature distribution, and the overall temperature of A: 40-50 is significantly reduced. Analyze the reasons, A: 10-20 has a small pore density, leading to a large radial resistance to the porous medium, which restricts the radial diffusion of high-temperature gas, and there is a large gradient in the radial temperature distribution. The layout of the porous media is A: 20-30; the pore density is the most suitable relative to the inlet parameters, and the radial and axial distribution ranges of the high temperature area are widened. As the pore density increases to A: 40-50, the overall combustor temperature drops drastically. Therefore, with Δn = 10 PPI, the temperature distribution is best at A: 20-30.

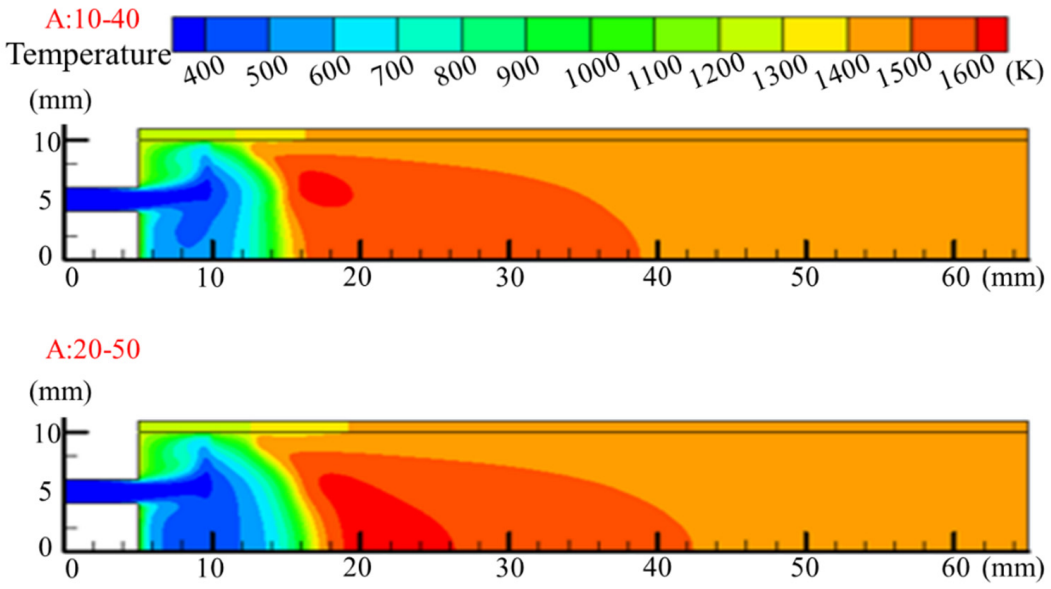

(**a**) Δn = 30 PPI

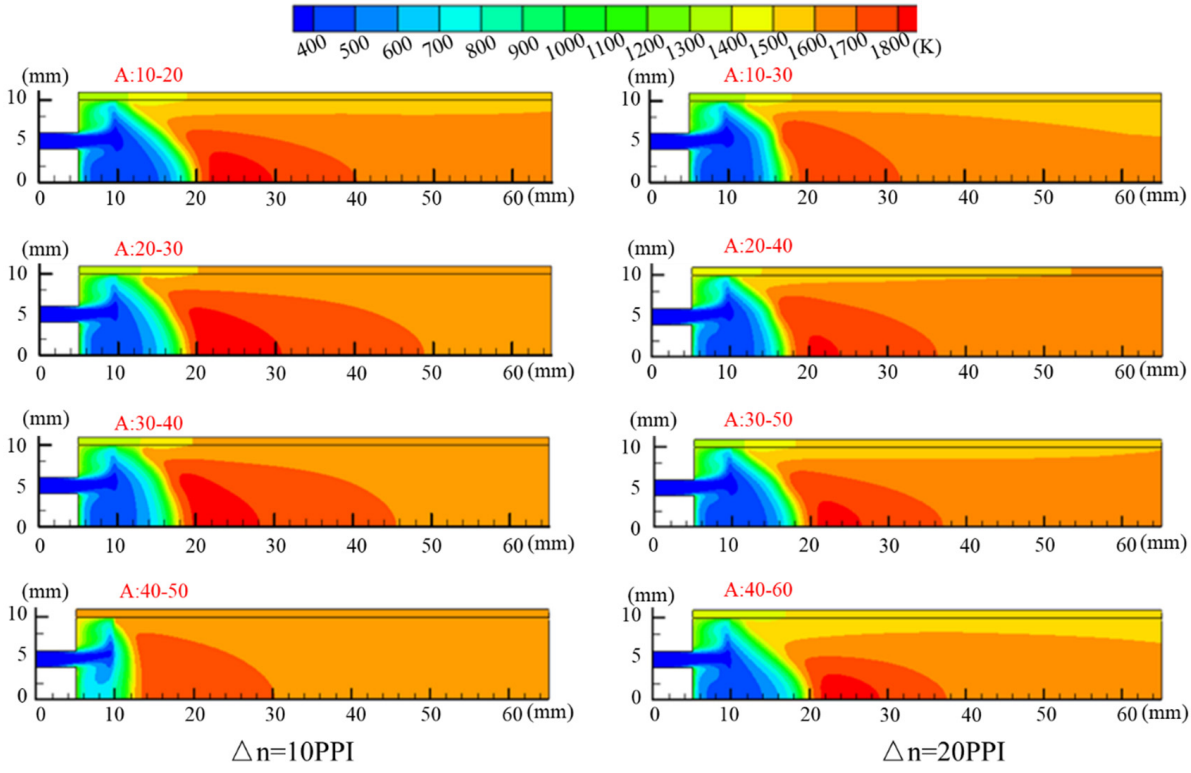

(**b**) Δn = 10 PPI and Δn = 20 PPI

Figure 11. Temperature distribution with different Δn.

Figure 12 shows the temperature distribution of the outer wall of the combustor at different Δn. Comprehensive comparison of the temperature distribution of the outer wall of the combustor when Δn is 10 PPI, 20 PPI, and 30 PPI, it is found that when Δn is 10 PPI, the highest wall temperature can reach 1570 K. Then Δn is 20 PPI, and the wall temperature is concentrated around 1550 K, as Δn increases to 30 PPI, the maximum wall temperature drops to 1360 K. It can be seen that Δn = 10 PPI is more reasonable, and it maintains excellent heat transfer performance. Detailed analysis of the outer wall temperature of the combustor when Δn = 10 PPI is shown in Figure 12a, four layouts are compared and

studied: A: 10-20, A: 20-30, A: 30-40, A: 40-50. The outer wall temperature of A: 10-20 can reach up to 1560 K, but A: 20-30 can reach 1570 K, with the increase of the pore size of the porous medium, the outer wall temperature has a downward trend. Overall layout A: 20-30 has the best outer wall temperature distribution, from a practical point of view, high outer wall temperature is often what we pursue, so A: 20-30 meets our requirements.

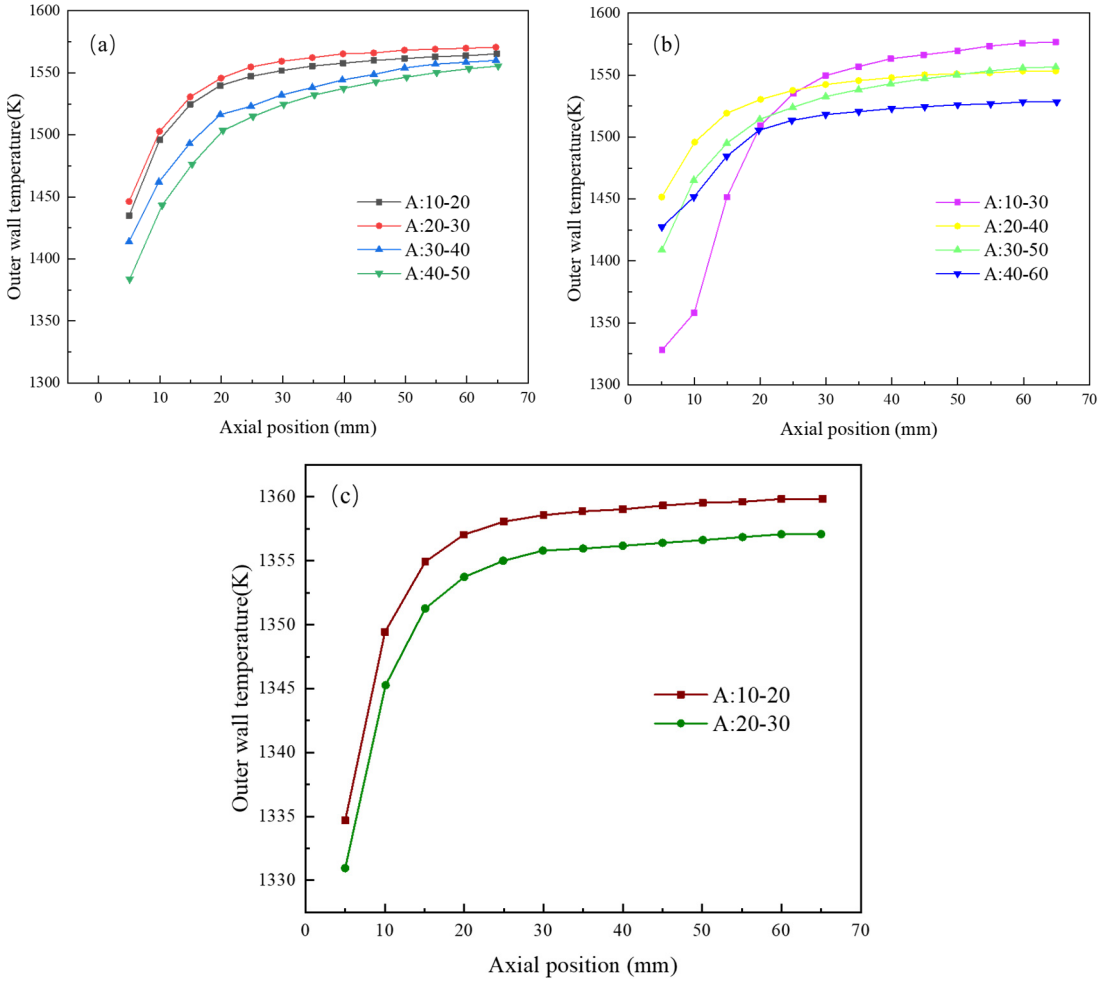

Figure 12. Outer wall temperature (**a**) Δn = 10 PPI, (**b**) Δn = 20 PPI, (**c**) Δn = 30 PPI.

Figure 13 shows the CH_4 conversion rate in the combustor for different Δn. Through comparative analysis of the CH_4 conversion rate of Figure 13a–c, it is found that when Δn is 10 PPI, the overall CH_4 conversion rate is relatively high, followed by 20 PPI, and the CH_4 conversion rate is significantly reduced at a Δn of 30 PPI. Therefore, it can be concluded that there should not be a large step in the void ratio between different porous media layers, and the methane conversion rate is higher when the increasing rate Δn is 10 PPI. Detailed comparison of the four layouts of Δn for 10 PPI, layouts A: 10-20, A: 20-30, A: 30-40, and A: 40-50 correspond to conversion efficiencies of 96.4%, 97.6%, 96.9%, and 96.8%, respectively. It can be seen that the conversion efficiency of A: 10-20 and A: 40-50 is relatively low, while A: 20-30 can still maintain a high conversion efficiency, so although a reasonable Δn is very important, the layout of porous media can further promote the efficient conversion of CH_4.

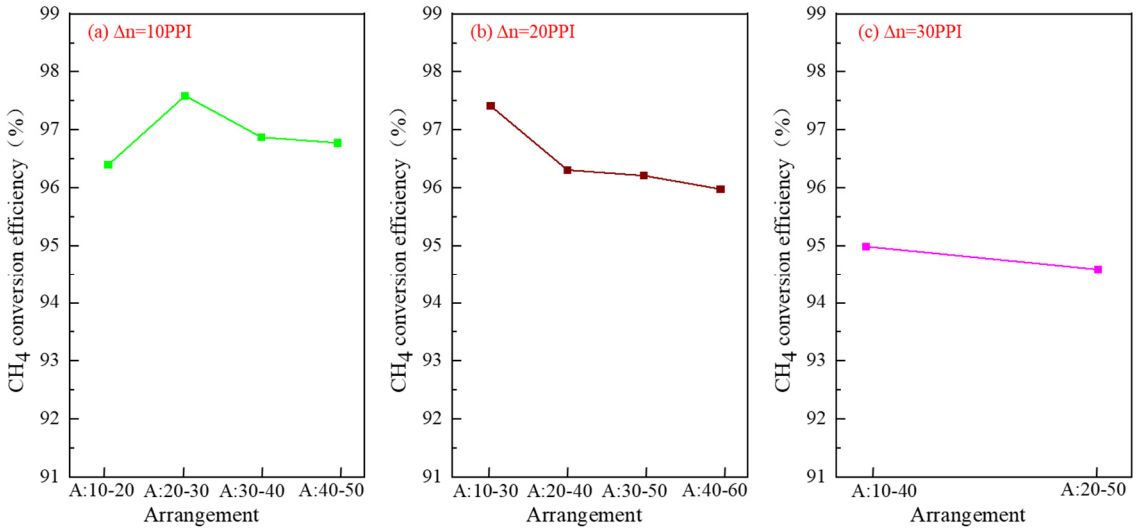

Figure 13. CH_4 conversion efficiency at different Δn.

3.4. Lean Flammable Limit

The previous research has determined various parameters of the porous medium of the combustor, but due to the good heat storage and heat transfer capabilities of the porous medium material, the porous medium combustor is suitable for lean combustion conditions. In addition, during fuel-rich combustion, over-temperature is prone to cause damage to the combustor. For example, when ϕ = 1.5, the highest temperature reaches 2400 K, which is higher than the melting point of Al_2O_3. Therefore, it is very necessary to study the lean flammable limit of the combustor, and three situations are selected to study the lean flammable limit in this paper. The first case is that the porous media is uniformly arranged, and the pore density is 20 PPI, named MC-U20. The second case is that the layout of porous media has been optimized, that is, the outer layer of large pore size and inner layer of small pore size porous media are arranged. Meanwhile, given the diameter ratio of the inner and outer layer d/D = 0.8, choose Δn = 20 PPI, the pore density of the porous medium is set to 10 PPI for the outer layer and 30 PPI for the inner layer, named MC-10/30-0.8. The third is the best parameter setting obtained from the previous optimization, the diameter ratio of the inner and outer layers is d/D = 0.5, the porosity increase rate of different porous media layers is Δn = 10 PPI, and the pore density is set to 20 PPI for the outer layer and 30 PPI for the inner layer, named MC-20/30-0.5. Selected the inlet velocity to be 0.5 m/s, 2.0 m/s, 3.5 m/s, and set the equivalent ratios of five lean combustion as ϕ = 0.2, ϕ = 0.3, ϕ = 0.4, ϕ = 0.5, ϕ = 0.6 for research.

As shown in Figure 14, the lean flammable limit range of different combustors is different. Figure 14a–c show the lean flammable limit distributions of MC-U20, MC-10/30-0.8, and MC-20/30-0.5, respectively. Since MC-U20, MC-10/30-0.8, and MC-20/30-0.5 are the optimization directions of our parameters, the lean flammable limit range increases successively, which is also consistent with our optimization research. For MC-U20, as the inlet velocity is 0.5 m/s, 2 m/s, and 3.5 m/s, the corresponding equivalent ratios are ϕ = 0.5, ϕ = 0.6, ϕ = 0.7, and the lowest lean flammable limit is ϕ = 0.5. The flammable limit of MC-10/30-0.8 maintains ϕ = 0.6 when the inlet velocity is 2 m/s and 3.5 m/s, but the lowest flammable limit can reach ϕ = 0.4 at 0.5 m/s. However, for MC-20/30-0.5, when the inlet velocity is 0.5 m/s, the lowest flammable limit can reach ϕ = 0.3, although at 3.5 m/s, its flammable limit can still be maintained at ϕ = 0.6. It can be seen that MC-20/30-0.5 has a lower flammable limit and brings better stability, which again proves that the structural parameters optimized above are reasonable. Therefore, the expansion of the lean combustible limit brings a larger lean burn range for combustion, avoiding the damage to the combustor under rich fuel conditions.

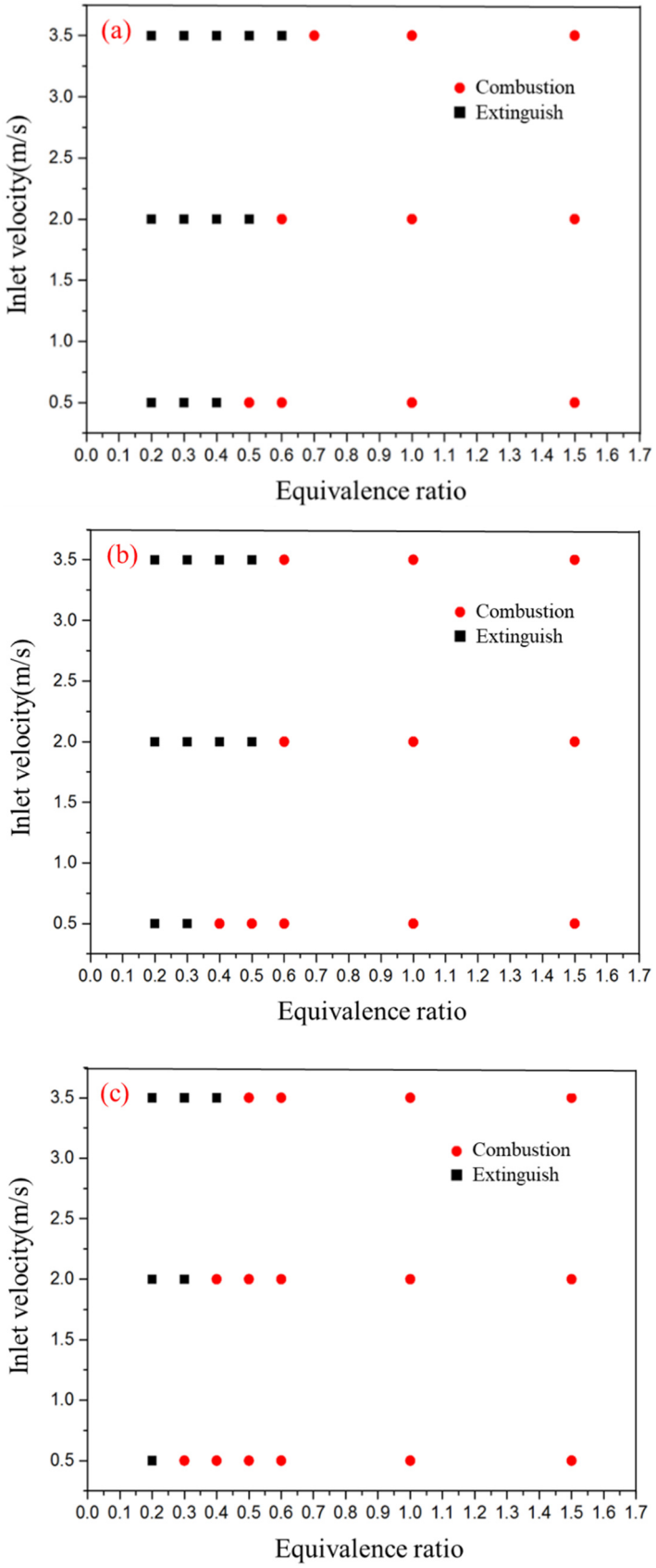

Figure 14. Lean flammable limit. (**a**) MC-U20, (**b**) MC-10/30-0.8, (**c**) MC-20/30-0.5.

4. Conclusions

This paper proposes to embed porous media in a combustor, studied the combustion characteristics of porous media through numerical simulation, and discusses and optimizes parameters such as porous media layout, d/D, increase rate, and lean flammable limit. The conclusions are as follows:

(1) The layout of porous media should be reasonable, and the small and large pore porous media embedded in the inner and outer layers can bring better combustion performance. A: 10-30 has a high and uniform temperature distribution, and its methane conversion rate has reached 97.4%, indicating that both combustion and heat transfer have been strengthened;

(2) The diameter ratio of the inner layer to the outer layer of the porous medium should be maintained at 0.4–0.6, which brings a more reasonable gas residence time, and further enables the pre-mixed gas to preheat and burn completely. At a d/D of 0.5, the combustor has the highest outer wall temperature and CH_4 conversion efficiency;

(3) Compared with the porosity gradient of Δn = 10 PPI, Δn = 10 PPI, the radial temperature distribution of the Δn = 10 PPI combustor is more uniform, and meanwhile it avoids the occurrence of local high temperature. Under the condition of Δn = 10 PPI, A: 20-30 layout has the highest outer wall temperature and CH_4 conversion efficiency;

(4) The lean flammable limits of MC-U20, MC-10/30-0.8, and MC-20/30-0.5 are compared, at an inlet velocity of 0.5 m/s, the corresponding lean flammable limits are 0.5, 0.4, and 0.3, respectively. Among them MC-20/30-0.5 has a wider flammable limit range, showing excellent combustion stability, which has a guiding significance for avoiding the destruction of the combustor under fuel-rich conditions.

The research in this article mainly focuses on the layout of porous media in the micro-combustor. However, there are some indicators that are of great research value and are expected to be further studied in future work. Typical examples include porous media materials, porous media resistance, pressure drop, and porous media structure.

Author Contributions: Writing—original draft preparation, F.W.; conceptualization, S.F.; writing—review and editing, F.W. and S.F.; supervision, X.L. and Y.Y.; funding acquisition, Y.Y. All authors have read and agreed to the published version of the manuscript.

Funding: The authors gratefully acknowledge financial support from Chongqing Special Equipment Inspection and Research Institute through the funds (No. CQTJKY202101), Chongqing Administration for Market Regulation through the funds (No. CQZJKY2018023) and the Graduate Scientific Research and Innovation Foundation of Chongqing (CYS21018).

Conflicts of Interest: The authors declare no conflict of interest.

References

1. E, J.; Ding, J.; Chen, J.; Liao, G.; Zhang, F.; Luo, B. Process in micro-combustion and energy conversion of micro power system: A review. *Energy Convers. Manag.* **2021**, *246*, 114664. [CrossRef]
2. Gharehghani, A.; Ghasemi, K.; Siavashi, M.; Mehranfar, S. Applications of porous materials in combustion systems: A comprehensive and state-of-the-art review. *Fuel* **2021**, *304*, 121411. [CrossRef]
3. Erdiwansyah, E.; Mahidin, M.; Husin, H.; Nasaruddin, N.; Muhtadin, M.; Faisal, M.; Gani, A.; Usman, U.; Mamat, R. Combustion Efficiency in a Fluidized-Bed Combustor with a Modified Perforated Plate for Air Distribution. *Processes* **2021**, *9*, 1489. [CrossRef]
4. He, Z.; Yan, Y.; Zhang, Z. Thermal management and temperature uniformity enhancement of electronic devices by micro heat sinks: A review. *Energy* **2020**, *216*, 119223. [CrossRef]
5. Xu, F.; Yan, Y.; He, Z.; Yang, Z.; Zhang, L. Numerical study on the influence of controllable flow ratio on combustion characteristics of a controllable central slotted bluff body and cavity combined micro combustor. *Int. J. Hydrogen Energy* **2021**, *46*, 6901–6914. [CrossRef]
6. He, Z.; Yan, Y.; Feng, S.; Li, X.; Fang, R.; Ou, Z.; Yang, Z. Numerical investigation on a multi-channel micro combustor fueled with hydrogen for a micro-thermophotovoltaic system. *Int. J. Hydrogen Energy* **2021**, *46*, 4460–4471. [CrossRef]
7. Wang, Y.; Zhang, M.; Chang, S.; Li, S.; Huang, X. Laser-Induced Ignition and Combustion Behavior of Individual Graphite Microparticles in a Micro-Combustor. *Processes* **2020**, *8*, 1493. [CrossRef]

8. Zhao, T.; Yan, Y.; He, Z.; Gao, W.; Yang, Z. Influence of hole size and number on pressure drop and energy output of the micro-cylindrical combustor inserting with an internal spiral fin with holes. *Int. J. Hydrogen Energy* **2021**, *46*, 26594–26606. [CrossRef]
9. Zhao, T.; Yan, Y.; He, Z.; Yang, Z. Influence of multi-structure optimization on the comprehensive performance of micro-cylindrical combustor inserting with spiral fin by using grey relational analysis and analysis of variance. *Int. J. Hydrogen Energy* **2021**, *46*, 28327–28337. [CrossRef]
10. Zhao, Z.; Wang, W.; Zuo, Z.; Kuang, N. Investigation on the flame characteristics of premixed propane/air in a micro opposed flow porous combustor. *Energy* **2022**, *238*, 121721. [CrossRef]
11. Li, Q.; Zuo, W.; Zhang, Y.; Li, J.; He, Z. Effects of rectangular rib on exergy efficiency of a hydrogen-fueled micro combustor. *Int. J. Hydrogen Energy* **2020**, *45*, 10155–10163. [CrossRef]
12. Benim, A.C.; Iqbal, S.; Meier, W.; Joos, F.; Wiedermann, A. Numerical investigation of turbulent swirling flames with validation in a gas turbine model combustor. *Appl. Therm. Eng.* **2017**, *110*, 202–212. [CrossRef]
13. Li, L.; Yang, G.; Fan, A. Non-premixed combustion characteristics and thermal performance of a catalytic combustor for micro-thermophotovoltaic systems. *Energy* **2021**, *214*, 118893. [CrossRef]
14. Yan, Y.; Wu, G.; Huang, W.; Zhang, L.; Li, L.; Yang, Z. Numerical comparison study of methane catalytic combustion characteristic between newly proposed opposed counter-flow micro-combustor and the conventional ones. *Energy* **2019**, *170*, 403–410. [CrossRef]
15. Pan, J.; Miao, N.; Lu, Z.; Lu, Q.; Yang, W.; Pan, Z.; Zhang, Y. Experimental and numerical study on the transition conditions and influencing factors of hetero-/homogeneous reaction for H_2/Air mixture in micro catalytic combustor. *Appl. Therm. Eng.* **2019**, *154*, 120–130. [CrossRef]
16. Landi, G.; Di Benedetto, A.; Barbato, P.S.; Russo, G.; Di Sarli, V. Transient behavior of structured $LaMnO_3$ catalyst during methane combustion at high pressure. *Chem. Eng. Sci.* **2014**, *116*, 350–358. [CrossRef]
17. Chen, J.; Yan, L.; Song, W.; Xu, D. Effect of heat and mass transfer on the combustion stability in catalytic micro-combustors. *Appl. Therm. Eng.* **2018**, *131*, 750–765. [CrossRef]
18. Di Benedetto, A.; Di Sarli, V.; Russo, G. A novel catalytic-homogenous micro-combustor. *Catal. Today* **2009**, *147*, S156–S161. [CrossRef]
19. Chen, J.; Song, W.; Gao, X.; Xu, D. Hetero-/homogeneous combustion and flame stability of fuel-lean propane–air mixtures over platinum in catalytic micro-combustors. *Appl. Therm. Eng.* **2016**, *100*, 932–943. [CrossRef]
20. Zhang, Y.; Pan, J.; Tang, A.; Liu, Y.; Pan, Z.; Lu, Q.; Otchere, P. Effect of gas-phase reaction on catalytic reaction for H_2/O_2 mixture in micro combustor. *Int. J. Hydrogen Energy* **2017**, *42*, 16855–16865. [CrossRef]
21. Chen, J.; Song, W.; Xu, D. Optimal combustor dimensions for the catalytic combustion of methane-air mixtures in micro-channels. *Energy Convers. Manag.* **2017**, *134*, 197–207. [CrossRef]
22. Jin, J.; Kwon, S. Fabrication and performance test of catalytic micro-combustors as a heat source of methanol steam reformer. *Int. J. Hydrogen Energy* **2010**, *35*, 1803–1811. [CrossRef]
23. Ipsakis, D.; Damartzis, T.; Papadopoulou, S.; Voutetakis, S. Dynamic Modeling and Control of a Coupled Reforming/Combustor System for the Production of H_2 via Hydrocarbon-Based Fuels. *Processes* **2020**, *8*, 1243. [CrossRef]
24. Zuo, W.; Zhang, Y.; Li, Q.; Li, J.; He, Z. Numerical investigations on hydrogen-fueled micro-cylindrical combustors with cavity for micro-thermophotovoltaic applications. *Energy* **2021**, *223*, 120098. [CrossRef]
25. Gao, W.; Yan, Y.; Huang, L.; Shen, K.; He, Z.; Gao, B. Numerical comparison of premixed H_2/air combustion characteristic of three types of micro cavity-combustors with guide vanes, bluff body, guide vanes and bluff body respectively. *Int. J. Hydrogen Energy* **2021**, *46*, 24382–24394. [CrossRef]
26. Su, Y.; Song, J.; Chai, J.; Cheng, Q.; Luo, Z.; Lou, C.; Fu, P. Numerical investigation of a novel micro combustor with double-cavity for micro-thermophotovoltaic system. *Energy Convers. Manag.* **2015**, *106*, 173–180. [CrossRef]
27. Yang, W.; Fan, A.; Yao, H. Effect of inlet temperature on combustion efficiency of lean H_2/air mixtures in a micro-combustor with wall cavities. *Appl. Therm. Eng.* **2016**, *107*, 837–843. [CrossRef]
28. He, Z.; Yan, Y.; Fang, R.; Ou, Z.; Zhang, Z.; Yang, Z.; Zhang, Z. Numerical investigation of a novel micro combustor with a central and bilateral slotted blunt body. *Int. J. Hydrogen Energy* **2021**, *46*, 23564–23579. [CrossRef]
29. Li, L.; Fan, A. A numerical study on non-premixed H_2/air flame stability in a micro-combustor with a slotted bluff-body. *Int. J. Hydrogen Energy* **2021**, *46*, 2658–2666. [CrossRef]
30. He, Z.; Yan, Y.; Xu, F.; Yang, Z.; Cui, H.; Wu, Z.; Li, L. Combustion characteristics and thermal enhancement of premixed hydrogen/air in micro combustor with pin fin arrays. *Int. J. Hydrogen Energy* **2020**, *45*, 5014–5027. [CrossRef]
31. Chakravarthy, S.; Randive, P. LES study on the effect of cavity configuration on combustion characteristics of a scramjet combustor with air-throttling. *Int. J. Hydrogen Energy* **2021**, *46*, 22534–22553. [CrossRef]
32. Suneetha, L.; Randive, P.; Pandey, K.M. Numerical investigation on implication of dual cavity on combustion characteristics in strut based scramjet combustor. *Int. J. Hydrogen Energy* **2019**, *44*, 32080–32094. [CrossRef]
33. Bao, H.; Zhou, J.; Pan, Y. Effect of cavity configuration on kerosene spark ignition in a scramjet combustor at Ma 4.5 flight condition. *Acta Astronaut.* **2015**, *117*, 368–375. [CrossRef]
34. Yang, H.-C.; Park, H.-O.; Park, K.-T.; Kim, S.-J.; Kim, H.-J.; Eun, H.-C.; Lee, K. Development of Carbonization and a Relatively High-Temperature Halogenation Process for the Removal of Radionuclides from Spent Ion Exchange Resins. *Processes* **2021**, *9*, 96. [CrossRef]

35. He, Z.; Yan, Y.; Feng, S.; Li, X.; Yang, Z.; Ran, J.; Gan, Y. Investigation on premixed methane/air combustion characteristics in heat recirculation micro combustor with separating cylinder. *Chem. Eng. Process.* **2020**, *153*, 107987. [CrossRef]
36. Tang, A.; Cai, T.; Huang, Q.; Deng, J.; Pan, J. Numerical study on energy conversion performance of micro-thermophotovoltaic system adopting a heat recirculation micro-combustor. *Fuel Process. Technol.* **2018**, *180*, 23–31. [CrossRef]
37. Tang, A.; Cai, T.; Deng, J.; Xu, Y.; Pan, J. Experimental investigation on combustion characteristics of premixed propane/air in a micro-planar heat recirculation combustor. *Energy Convers. Manag.* **2017**, *152*, 65–71. [CrossRef]
38. Yedala, N.; Kaisare, N.S. A CFD study of ignition of lean propane-air mixtures in a heat recirculating U-bend catalytic microreactor. *Chem. Eng. Res. Des.* **2021**, *173*, 15–26. [CrossRef]
39. Di Sarli, V. The Effect of Differentiating the Thermal Conductivity between Inner and Outer Walls on the Stability of a U-Bend Catalytic Heat-Recirculating Micro-Combustor: A CFD Study. *Appl. Sci.* **2021**, *11*, 5418. [CrossRef]
40. Ma, L.; Fang, Q.; Zhang, C.; Chen, G. A novel Swiss-roll micro-combustor with double combustion chambers: A numerical investigation on effect of solid material on premixed CH_4/air flame blow-off limit. *Int. J. Hydrogen Energy* **2021**, *46*, 16116–16126. [CrossRef]
41. Variny, M.; Varga, A.; Rimár, M.; Janošovský, J.; Kizek, J.; Lukáč, L.; Jablonský, G.; Mierka, O. Advances in Biomass Co-Combustion with Fossil Fuels in the European Context: A Review. *Processes* **2021**, *9*, 100. [CrossRef]
42. Wu, Y.; Peng, Q.; Yang, M.; Shan, J.; Yang, W. Entropy generation analysis of premixed hydrogen–air combustion in a micro combustor with porous medium. *Chem. Eng. Process.* **2021**, *168*, 108566. [CrossRef]
43. Ni, S.; Zhao, D.; Cai, T.; Cao, F. Energy conversion efficiency improvement studies on unconventional premixed micro-combustors partially inserted with porous medium. *Fuel Process. Technol.* **2021**, *215*, 106774. [CrossRef]
44. Peng, Q.; Yang, W.; Jiaqiang, E.; Xu, H.; Li, Z.; Tay, K.; Zeng, G.; Yu, W. Investigation on premixed H_2/C_3H_8/air combustion in porous medium combustor for the micro thermophotovoltaic application. *Appl. Energy* **2020**, *260*, 114352. [CrossRef]
45. Peng, Q.; Xie, B.; Yang, W.; Tang, S.; Li, Z.; Zhou, P.; Luo, N. Effects of porosity and multilayers of porous medium on the hydrogen-fueled combustion and micro-thermophotovoltaic. *Renew. Energy* **2021**, *174*, 391–402. [CrossRef]
46. Li, J.; Wang, Y.; Shi, J.; Liu, X. Dynamic behaviors of premixed hydrogen–air flames in a planar micro-combustor filled with porous medium. *Fuel* **2015**, *145*, 70–78. [CrossRef]
47. Wang, W.; Zuo, Z.; Liu, J. Numerical study of the premixed propane/air flame characteristics in a partially filled micro porous combustor. *Energy* **2019**, *167*, 902–911. [CrossRef]
48. Quaye, E.K.; Pan, J.; Zhang, Y.; Lu, Q.; Wang, Y.; Alubokin, A.A. Effects of influencing factors on premixed CH_4-O_2 combustion in a cylindrical porous media combustor. *Chem. Eng. Process.* **2021**, *161*, 108320. [CrossRef]
49. Pan, J.F.; Wu, D.; Liu, Y.X.; Zhang, H.F.; Tang, A.K.; Xue, H. Hydrogen/Oxygen Premixed Combustion Characteristics in Micro Porous Media Combustor. *Energy Procedia* **2014**, *61*, 1279–1285. [CrossRef]
50. Wang, Y.; Shi, Y.; Cao, T.; Zeng, H.; Cai, N.; Ye, X.; Wang, S. A flame fuel cell stack powered by a porous media combustor. *Int. J. Hydrogen Energy* **2018**, *43*, 22595–22603. [CrossRef]
51. Pedras, M.H.J.; de Lemos, M.J.S. Thermal dispersion in porous media as a function of the solid–fluid conductivity ratio. *Int. J. Heat Mass Transf.* **2008**, *51*, 5359–5367. [CrossRef]
52. Pedras, M.H.J.; de Lemos, M.J.S. Macroscopic turbulence modeling for incompressible flow through undeformable porous media. *Int. J. Heat Mass Transf.* **2001**, *44*, 1081–1093. [CrossRef]
53. Ma, P.; Tang, Z.; Cai, W. An experimental study and modeling on the flow resistance of airflow through foam ceramic. *Nat. Gas Ind.* **2010**, *30*, 97–101.
54. Wan, J.; Fan, A.; Yao, H.; Liu, W. Effect of thermal conductivity of solid wall on combustion efficiency of a micro-combustor with cavities. *Energy Convers. Manag.* **2015**, *96*, 605–612. [CrossRef]
55. Kuo, C.H.; Ronney, P.D. Numerical modeling of non-adiabatic heat-recirculating combustors. *Proc. Combust. Inst.* **2007**, *31*, 3277–3284. [CrossRef]
56. Wan, J.; Yang, W.; Fan, A.; Liu, Y.; Yao, H.; Liu, W.; Du, Y.; Zhao, D. A numerical investigation on combustion characteristics of H_2/air mixture in a micro-combustor with wall cavities. *Int. J. Hydrogen Energy* **2014**, *39*, 8138–8146. [CrossRef]
57. Wang, E.; Cheng, L.; Luo, Z.; Cen, K.F. Experimental study on the temperature profiles of premixed combustion in a gradually-varied porous medium. *J. Therm. Sci. Technol.* **2003**, *2*. [CrossRef]